

Preprint Series

Fast Multipole Method for Poroelastodynamics

Martin Schanz

Institute of Applied Mechanics, Graz University of Technology

Published in *Engineering Analysis with Boundary Elements*, 89, 50–59,
2018

DOI: 10.1016/j.enganabound.2018.01.014

Latest revision: December 21, 2017

Abstract

Wave propagation phenomena occur in reality often in semi-infinite two-phase (porous) regions. It is well known that such problems can be handled well with the poroelastodynamic Boundary Element Method (BEM). But, it is also well known that the BEM with its dense matrices becomes prohibitive with respect to storage and computing time. This is especially true for poroelastodynamics, where in the best case four degrees of freedom per node are required. As well, the fundamental solution of poroelastodynamics is computationally expensive.

Here, a fast multipole BEM is proposed to circumvent those points. The Chebyshev interpolation-based FMM significantly reduces the memory consumption of the system matrix and thus allows for larger problem sizes to be treated. As well, it requires fewer evaluations of the fundamental solution. To employ an iterative solver, the use of a transformation of the material data is mandatory. Numerical tests show the expected almost linear complexity of the proposed method.

1 Introduction

Porous media occur frequently in nature as well as construction materials. Probably, the best-known example for a natural porous medium is soil. The understanding of wave propagation in such media is of distinct interest for oil and gas exploration but also for earthquake analysis. In these particular fields the treatment of unbounded domains, such as a halfspace, is required. The Boundary Element Method (BEM) is advantageous over the Finite Element Method (FEM) for the numerical treatment of such geometries, since it requires only the discretisation of the boundary and inherently fulfills the radiation condition. A review of poroelastic models and their numerical treatment is given in [40].

Based on the work of von Terzaghi, a theoretical description of porous materials saturated by a viscous fluid was presented by Biot [5]. In the following years, Biot extended his theory to anisotropic cases [6] and also to poroviscoelasticity [9]. To treat wave propagation a dynamic theory is necessary, which can be found in two papers, one for low frequency range [7] and the other for high frequency range [8]. Alternatively, the theory of porous media (TPM) can be used, which goes back to Fillunger and has been brought to a mature state by de Boer [15] and Ehlers [18, 19]. The dynamic extension of the TPM can be found in [16]. Assuming a linear geometrical and a linear constitutive model, a comparison of both theories has been published by Schanz and Diebels [41], which shows that the mathematical operator of both theories is the same. This has the physical consequence that in both theories three waves exist, two compressional waves and one shear wave. The numerical consequence is that all methods can be transferred from one theory to the other as long as the linear description holds.

As already written above, here the focus is on a boundary element formulation. First poroelastodynamic BE formulations based on Biot's theory have been published in Laplace domain by Manolis and Beskos [30] expressed in terms of solid and fluid displacements. However, it can be shown that only the solid displacements and one additional variable, the fluid pressure, are independent [10]. Formulations in frequency domain have been published by Cheng et al. [14] and Domínguez [17] based on these unknowns. A time domain formulation was developed by Wiebe and Antes [48], but with the restriction of vanishing damping between the solid skeleton and the fluid. Another time dependent formulation was proposed by Chen and Dargush based on analytical inverse transformation of the Laplace domain fundamental solutions [13]. Utilizing the convolution quadrature method [28, 29] a time stepping based BE formulation has been proposed by Schanz [38, 39]. The latter formulation uses the Laplace domain fundamental solutions but works in time domain. Hence, all regularization techniques known for the elliptic operator can be applied, which has been done in [32]. All the above mentioned formulations are based on the first integral equation and the collocation method. A symmetric Galerkin based formulation has been presented by Messner and Schanz [33] and a mathematical analysis of the Laplace domain version can be found in [43].

The above mentioned BE-formulations have a quadratic complexity in the spatial variable. Hence, for real world problems the effort becomes prohibitive. To overcome this drawback so-called fast methods have become popular in the field of applied mathematics and engineering. The history of such methods, i.e., asymptotically optimal approximations of dense matrices, starts with the paper by Rokhlin [37]. For the first time an algorithm was presented which scales like $O(n \log n)$. Subsequently, the so called Fast Multipole Method (FMM) has been developed

in [22] for some large-scale n-body problems. The method was significantly improved in [23]. In the work of Of et al. [36] the FMM is applied to elastostatic problems based on a Galerkin BEM discretization. The extension to elastodynamics in Fourier domain has been published in [12] based on a collocation approach. In time domain, the FMM with a plane wave expansion is presented in [44]. A textbook on the FMM with application in collocation BEM has been published by Liu [27] and a literature review can be found in [35].

Another approach is the wavelet based BEM [1], which produces sparse matrices based on orthogonal systems of wavelet like functions. On a purely algebraic level works the Adaptive Cross Approximation (ACA), which has been proposed by Bebendorf [2], Bebendorf and Rjasanow [4]. The latter fast method is often classified as black-box method, because the ACA is (nearly) independent of the kernel function. An application to the Galerkin BEM in elastostatics can be found in [3]. Other black-box methods for a FMM uses a series expansion of the kernel and can in this sense also be classified as black-box. The Panel Clustering (see [24]) is the first of these methods. A refined version, where the kernel expansion is based on a Chebyshev interpolation, has been published by Fong and Darve [21]. The extension of this approach to acoustics with a directional clustering is presented in [34]. The advantage of these black-box methods against the usual FMM is that no analytical kernel expansion has to be known. However, the price to pay is usually a higher complexity which is still almost linear but the expansion order of the kernel enters with a power of six in 3-d instead of four using, e.g., spherical harmonics for the Helmholtz kernel. But for poroelastodynamics this black-box property is essential as no analytic kernel expansion seems to be possible. There might be a possibility to reduce the kernel to a combination of derivatives of the Helmholtz kernel as it has been done in [12] for elastodynamics. However, this requires to shift some derivatives to the interpolation polynomials, which increases the necessary polynomial order, and a lot of analytical preparations of the kernel. A study on these different approaches can be found for elastodynamics in the thesis [45].

Here, a FMM based on a Chebyshev interpolation will be presented for poroelastodynamics in Laplace domain. For an uncoupled quasistatic poroelastic problem the same FMM idea has been applied in [47]. The presented Laplace domain formulation includes also problems in Fourier/frequency domain if the real part of the Laplace variable is set to zero. The idea is to use the whole vectorial kernel within the Chebyshev interpolation of the kernel. This results in vectorial M2L-operators but avoids to high interpolation orders. Further, the method is nearly black-box and can use already coded functions for the evaluation of the kernel.

The paper is organized as follows. First, the basic equations and the corresponding integral equations are recalled. The FMM is given in section 3 in a short way because it is only an extension from the algorithm given by Fong and Darve [21]. The modifications necessary for the vectorial kernel of poroelastodynamics will be discussed. The proposed formulation is then tested in section 4.

Throughout this paper, vectors and tensors are denoted by bold symbols and matrices and vectors of the discretised system by upper case and lower case sans serif symbols, respectively. No summation convention is used in the entire work. The indices of a matrix $(A)_{ij}$ indicate the ij -th entry, which might be a scalar or a matrix value.

2 Governing equations

Following Biot's approach to model the behavior of a porous media, an elastic skeleton with a statistical distribution of interconnected pores is considered [6]. This porosity is denoted by ϕ , which is the relation of the volume of the interconnected pores to the bulk volume. Contrary to these pores the sealed pores will be considered as part of the solid. Full saturation is assumed, i.e., a two-phase material is given. Assuming compressible constituents, a linear elastic solid skeleton, and a linear geometrical description results in a set of coupled partial differential equations (for details see [7]). The problem can be given as follows.

2.1 Problem setting

Let $\Omega \subset \mathbb{R}^3$ be a bounded Lipschitz domain and $\Gamma := \partial\Omega$ its boundary with the outward normal \mathbf{n} . The coupled set of homogeneous partial differential equation for the solid displacements $\mathbf{u}(\mathbf{x})$ and the pore pressure $p(\mathbf{x})$ are considered

$$\begin{aligned} G\nabla\nabla\mathbf{u}(\mathbf{x}) + \left(K + \frac{1}{3}G\right)\nabla\nabla\cdot\mathbf{u}(\mathbf{x}) - s^2(\rho - \beta\rho_f)\mathbf{u}(\mathbf{x}) - (\alpha - \beta)\nabla p(\mathbf{x}) &= 0 \\ \frac{\beta}{s\rho_f}\nabla^2 p(\mathbf{x}) - \frac{\phi^2 s}{R}p(\mathbf{x}) - (\alpha - \beta)s\nabla\cdot\mathbf{u}(\mathbf{x}) &= 0 \end{aligned} \quad \forall \mathbf{x} \in \Omega \quad (1)$$

with the parameter

$$\beta = \frac{\kappa\rho_f\phi^2 s}{\phi^2 + s\kappa(\rho_a + \phi\rho_f)} \quad \text{and} \quad \rho_a = 0.66\phi\rho_f.$$

It is assumed that the pore pressure and the solid displacements are in Laplace domain with the Laplace variable $s \in \mathbb{C}$ s.t. $\Re s > 0$. The used material data are the shear and bulk modulus of the skeleton, G and K . The bulk density $\rho = (1 - \phi)\rho_s + \phi\rho_f$ is the weighted combination of the solid density ρ_s and the fluid density ρ_f . The Biot parameters are denoted by R and α , where the latter describes the compressibility of the solid grains (i.e., $\alpha = 1$ is the incompressible limit). The spatial derivatives are given with the ∇ -operator with its usual meanings as $\text{grad} = \nabla$ or $\text{div} = \nabla\cdot$. The assumption for the apparent mass density ρ_a holds for low frequencies [11]. For different materials the factor 0.66 might be different and a certain frequency dependency can be added [8]. Further, for higher frequencies as well the permeability should be modelled as a function of s [25], which does not change the subsequent derivation. However, the proposed FMM will be restricted to low frequencies and, consequently, here the dependency is skipped. The boundary is split into non-overlapping sets Γ_D and Γ_N such that $\Gamma = \Gamma_D \cup \Gamma_N$ holds. The Dirichlet and Neumann boundary conditions are given by

$$\begin{aligned} \mathbf{u}(\mathbf{x}) &= \mathbf{f}_D(\mathbf{x}) \quad \forall \mathbf{x} \in \Gamma_D \\ p(\mathbf{x}) &= g_D(\mathbf{x}) \quad \forall \mathbf{x} \in \Gamma_D \\ \mathbf{t}(\mathbf{x}) = \mathcal{T}^S\mathbf{u}(\mathbf{x}) - \alpha\mathbf{n}p(\mathbf{x}) &= \mathbf{f}_N(\mathbf{x}) \quad \forall \mathbf{x} \in \Gamma_N \\ q(\mathbf{x}) = -\frac{\beta}{s\rho_f} \left(\frac{\partial}{\partial \mathbf{n}} p(\mathbf{x}) + \rho_f s^2 \mathbf{n}^\top \cdot \mathbf{u}(\mathbf{x}) \right) &= g_N(\mathbf{x}) \quad \forall \mathbf{x} \in \Gamma_N, \end{aligned} \quad (2)$$

where $\mathbf{t}(\mathbf{x})$ is the total traction vector and $q(\mathbf{x})$ the flux. In (2), the elastic traction operator

$$\mathcal{T}^S \bullet = \left(K - \frac{2}{3}G \right) \mathbf{n} \nabla \cdot \bullet + 2G \frac{\partial}{\partial \mathbf{n}} \bullet + G \mathbf{n} \times (\nabla \times \bullet) \quad (3)$$

has been used. The given set of partial differential equations is the so-called u - p -formulation, which needs only four (in 3D) degrees of freedom (dofs). There exists also formulations for poroelastic continua with more dofs, which are formulated with the solid and fluid displacements or even with the latter both and the pore pressure. However, for linear problems the proposed one is sufficient and has the minimum amount of dofs [10]. Certainly, the boundary condition type, Dirichlet or Neumann, might differ in each direction of the vectorial dofs and between the elastic and fluid dofs. However, for simplifying notation this is not separately denoted. Also it should be remarked that all variables are in Laplace domain as noted above. A frequency domain formulation is automatically included by setting the real part of s to zero.

As already reported in [13] for a reliable numerical method dimensionless variable should be introduced. Based on the suggestion in [13] a study on different versions of dimensionless variables have been performed in [42]. The latter suggest as minimal set the following scaling of the material data

$$\tilde{K} = \frac{K}{C} \quad \tilde{G} = \frac{G}{C} \quad \tilde{\rho} = \frac{\rho}{C} \quad \tilde{\kappa} = C\kappa \quad \text{with } C = \frac{9KG}{3K+G}. \quad (4)$$

Essentially, all material data are scaled to the Young's modulus of the elastic skeleton. This choice is used in the subsequent given BE formulations, which allows to use an iterative solver. This is a minimum requirement for an FMM.

2.2 Boundary integral formulations

Indirect and direct boundary integral formulations are possible. The latter are the more common version in engineering (see, e.g., [14, 39]) but the first are often used in the mathematical literature. Here, three versions are given without any derivation as this can be found in literature (see for a direct formulation, e.g., [13, 39]). The motivation for the indirect formulation is to have a suitable tool to test each operator separately. For the correct mathematical setting the reader is directed to [46].

For a short notation the vector of generalized displacements $\mathbf{u}^g = (\mathbf{u}, p)^\top$ and generalized tractions $\mathbf{t}^g = (\mathbf{t}, q)^\top$ is introduced. It simply summarizes the respective dofs in one vector. The fundamental solutions of the governing equations (1), i.e., the solution of the adjoint operator, are denoted by

$$\mathbf{U}(\mathbf{x}, \mathbf{y}) = \begin{pmatrix} U^S & U^f \\ -P^S & -P^f \end{pmatrix}, \quad (5)$$

with U^S being a three-by-three tensor, U^f a three-by-one tensor, P^S a one-by-three tensor, and P^f a scalar. The explicit expressions of the four subblocks can be found in [38]. Further, the poroelastic adjoint traction operator is defined with

$$\mathcal{T}_y = \begin{pmatrix} \mathcal{T}_y^S & -s \boldsymbol{\alpha} \mathbf{n}_y \\ -\boldsymbol{\beta} \mathbf{n}_y^\top & -\frac{\beta}{s\rho^f} \frac{\partial}{\partial \mathbf{n}_y} \end{pmatrix}. \quad (6)$$

The index at the elastic traction operator \mathcal{T}_y^S and at the normal vector is set to specify the point of evaluation.

With these notations the integral equations can be given. A solution $\mathbf{u}^g(\mathbf{x})$ for $\mathbf{x} \in \Omega$ can be constructed by the indirect single layer potential (SLP) approach

$$\mathbf{u}^g(\mathbf{x}) = \int_{\Gamma} (\mathbf{U}(\mathbf{x}, \mathbf{y}))^\top \mathbf{w}(\mathbf{y}) \, ds_{\mathbf{y}} \quad \forall \mathbf{x} \in \Omega, \quad (7)$$

or by the double layer potential (DLP) approach

$$\mathbf{u}^g(\mathbf{x}) = \int_{\Gamma} (\mathcal{T}_y \mathbf{U}(\mathbf{x}, \mathbf{y}))^\top \mathbf{v}(\mathbf{y}) \, ds_{\mathbf{y}} \quad \forall \mathbf{x} \in \Omega. \quad (8)$$

The functions $\mathbf{w}(\mathbf{y})$ and $\mathbf{v}(\mathbf{y})$ are density functions to be determined by the boundary condition. For this purpose (7) and (8) has to be evaluated at the boundary, for which the trace operator is applied. The corresponding boundary integral equations are after careful considerations of the singularities of the fundamental solutions

$$\mathbf{u}^g(\mathbf{x}) = \int_{\Gamma} (\mathbf{U}(\mathbf{x}, \mathbf{y}))^\top \mathbf{w}(\mathbf{y}) \, ds_{\mathbf{y}} \quad \forall \mathbf{x} \in \Gamma \quad (9)$$

and

$$\mathbf{u}^g(\mathbf{x}) = \int_{\Gamma} (\mathcal{T}_y \mathbf{U}(\mathbf{x}, \mathbf{y}))^\top \mathbf{v}(\mathbf{y}) \, ds_{\mathbf{y}} + (\mathcal{C}(\mathbf{x}) - I) \mathbf{v}(\mathbf{x}) \quad \forall \mathbf{x} \in \Gamma. \quad (10)$$

Formally, the integral over the upper left block of $(\mathcal{T}_y \mathbf{U}(\mathbf{x}, \mathbf{y}))^\top$ has to be defined as Cauchy Principal value. The integral free term in (10) is a combination of the well known terms from elastostatics and the Laplace operator put on the main diagonal. It is formally

$$\mathcal{C}(\mathbf{x}) = \lim_{\varepsilon \rightarrow 0} \int_{\mathbf{y} \in \Omega: |\mathbf{y} - \mathbf{x}| = \varepsilon} (\mathcal{T}_y \mathbf{U}(\mathbf{y} - \mathbf{x}))^\top \, ds_{\mathbf{y}}. \quad (11)$$

Details can be found in [32]. There also a regularization strategy is discussed, which is based on partial integration resulting in only weakly singular integrals. As in the following numerical tests only Dirichlet problems are treated, the above indirect approaches are sufficient. The extension to Neumann problems is straight forward.

For mixed problems the direct approach will be used. The representation formula for the direct approach is a combination of the SLP and the DLP operator but both are applied on physical quantities. The derivation can be made either via a reciprocal work theorem or starting from a weighted residual statement (see, e.g., [17, 38]). Finally, for points in the domain it is

$$\mathbf{u}^g(\mathbf{x}) = \int_{\Gamma} \left[(\mathbf{U}(\mathbf{x}, \mathbf{y}))^\top \mathbf{t}^g(\mathbf{y}) - (\mathcal{T}_y \mathbf{U}(\mathbf{x}, \mathbf{y}))^\top \mathbf{u}^g(\mathbf{y}) \right] \, ds_{\mathbf{y}} \quad \forall \mathbf{x} \in \Omega, \quad (12)$$

and on the boundary

$$C(\mathbf{x}) \mathbf{u}^g(\mathbf{x}) = \int_{\Gamma} \left[(\mathbf{U}(\mathbf{x}, \mathbf{y}))^\top \mathbf{t}^g(\mathbf{y}) - (\mathcal{T}_y \mathbf{U}(\mathbf{x}, \mathbf{y}))^\top \mathbf{u}^g(\mathbf{y}) \right] d s_y \quad \forall \mathbf{x} \in \Gamma. \quad (13)$$

Based on the above mentioned regularization the boundary integral equation (13) can be cast into a only weakly singular representation.

2.3 Spatial discretization

The computational domain Γ is approximated by a standard triangulation with only flat linear triangles. This results in the discretized boundary

$$\Gamma \approx \Gamma_h = \bigcup_{k=1}^K \tau_k \quad (14)$$

as the union of K triangles τ_k . The solutions $\mathbf{u}^g, \mathbf{t}^g$ and the densities \mathbf{v}, \mathbf{w} are approximated using constant discontinuous functions φ^0 for

$$\mathbf{w}(\mathbf{x}) \approx \sum_{j=1}^N \varphi_j^0(\mathbf{x}) \mathbf{w}_j \quad \mathbf{t}^g(\mathbf{x}) \approx \sum_{j=1}^N \varphi_j^0(\mathbf{x}) \mathbf{t}_j^g \quad (15)$$

and using linear continuous functions φ^1 for

$$\mathbf{v}(\mathbf{x}) \approx \sum_{j=1}^M \varphi_j^1(\mathbf{x}) \mathbf{v}_j \quad \mathbf{u}^g(\mathbf{x}) \approx \sum_{j=1}^M \varphi_j^1(\mathbf{x}) \mathbf{u}_j^g, \quad (16)$$

respectively. Note that for the vector valued problem at hand, the coefficients $\mathbf{w}_j, \mathbf{t}_j^g, \mathbf{v}_j$, and \mathbf{u}_j^g are accordingly vector valued. The supports of the functions are restricted to either one or several neighboring triangles. This yields either N or M unknowns. To set up a system of equations a collocation method is employed. The collocation is either performed at the mid node of the element for those unknowns approximated by constant shape functions or at the nodes of the triangle for those unknowns approximated by linear shape functions. This collocation procedure can be written for the SLP approach as

$$\mathbf{u}^g(\mathbf{x}_i) = \sum_{j=1}^N \int_{\text{supp}(\varphi_j^0)} (\mathbf{U}(\mathbf{x}_i, \mathbf{y}))^\top \varphi_j^0(\mathbf{y}) d s_y \mathbf{w}_j =: \sum_{j=1}^N V_{ij} \mathbf{w}_j \quad (17)$$

and for the DLP approach as

$$\mathbf{u}^g(\mathbf{x}_i) = \sum_{j=1}^M \int_{\text{supp}(\varphi_j^1)} (\mathcal{T}_y \mathbf{U}(\mathbf{x}_i, \mathbf{y}))^\top \varphi_j^1(\mathbf{y}) d s_y \mathbf{v}_j + (C(\mathbf{x}_i) - I) \mathbf{v}(\mathbf{x}_i) =: \sum_{j=1}^M (K_{ij} + (C_{ij} - \delta_{ij})) \mathbf{v}_j. \quad (18)$$

Note that the indices i, j refer to four-by-four blocks of the fundamental solution and to a sub-vector w_j of length four. For all collocation points the matrix entries of (17) or (18) constitute the equation system to be solved. After finding the densities the discretized versions of (7) and (8) gives the physical quantities either on the boundary or inside the domain.

For the direct approach the discretized integral equation is

$$C(\mathbf{x}_i) \mathbf{u}_i^g = \sum_{j=1}^N \int_{\text{supp}(\varphi_j^0)} (\mathbf{U}(\mathbf{x}_i, \mathbf{y}))^\top \varphi_j^0(\mathbf{y}) d.s_{\mathbf{y}} \mathbf{t}_j^g - \sum_{j=1}^M \int_{\text{supp}(\varphi_j^1)} (\mathcal{T}_{\mathbf{y}} \mathbf{U}(\mathbf{x}_i, \mathbf{y}))^\top \varphi_j^1(\mathbf{y}) d.s_{\mathbf{y}} \mathbf{u}_j^g. \quad (19)$$

The collocation is performed either on the mid node of the element, if this is a Neumann boundary, or the nodes of the triangles, if this is a Dirichlet boundary. The whole discrete system must be rearranged according to the known and unknown boundary data to obtain finally

$$\begin{bmatrix} V_{DD} & -K_{DN} \\ V_{ND} & -(C_{NN} + K_{NN}) \end{bmatrix} \begin{bmatrix} \mathbf{t}_D^g \\ \mathbf{u}_N^g \end{bmatrix} = \begin{bmatrix} C_{DD} + K_{DD} & -V_{DN} \\ K_{ND} & -V_{NN} \end{bmatrix} \begin{bmatrix} \mathbf{g}_D \\ \mathbf{g}_N \end{bmatrix}. \quad (20)$$

In (20), all given Dirichlet data \mathbf{f}_D and g_D are collected in \mathbf{g}_D and all given Neumann data \mathbf{f}_N and g_N in \mathbf{g}_N according to the collocation points. The partitioning of the system matrices with respect to the collocation point and the element to be integrated is indicated by the indices D and N .

For all above given BE formulations the regularization has been performed with partial integration as published in [32]. The remaining weakly singular integrals are solved numerically with the formulas of Erichsen and Sauter [20]. All regular integrals are performed with Gaussian quadrature formulas.

3 Fast multipole method

The above presented BE formulations (17) for the indirect SLP approach, (18) for the DLP approach, and (20) for the direct approach are ready to be solved for specific problems. The final system of equations are usually solved for small problem sizes with a direct solver like the LU-decomposition. For larger problem sizes iterative solvers like the GMRes are often used to reduce the effort to a quadratic complexity. As already discussed in the introduction, the matrix-vector product used in iterative solvers can be accelerated with the Fast Multipole Method. The basic idea of the FMM is to construct a fast summation scheme by the use of a low rank representation of the kernel. To put it simply, the dependency of the fundamental solution on the distance $|\mathbf{x} - \mathbf{y}|$ is changed to a dependency on the product of two functions depending each only on either \mathbf{x} or \mathbf{y} .

The FMM used here is a Chebyshev interpolation-based FMM based on the blackbox FMM presented by Fong and Darve [21]. Indeed, the blackbox feature is used here, i.e., the formulation presented by Fong and Darve [21] can be used nearly as presented in this paper. The three discussed BE formulations uses either the discretized boundary integral operator V_{ij} or K_{ij} , or a combination of both. Thus, it involves the integration over the kernel and the low rank representation of it, i.e., the separation of the field and load point allows to shift its evaluation outside the integral. The low rank representation of the kernel introduces acceptable errors only

for distant points \mathbf{x}, \mathbf{y} , i.e., for off-diagonal blocks of the system matrix. To get a separation of the geometry in near field (for the normal kernel) and a far field (for the low rank kernel) the standard geometrical clustering scheme of the FMM (see, e.g., [27]) is employed. This is as well the basis of a multilevel schema. For the FMM-BEM the clustering goes over the collocation points, which is straightforward, and over the shape functions. Because of the strictly geometrical clustering the supports of some shape functions are not entirely enclosed within the cluster's boundaries. Thus the cluster's bounding box is extended such that the supports are just enclosed within. Note that for the DLP approach linear continuous shape functions are employed to approximate the density, while constant discontinuous shape functions are used for the SLP approach, resulting in different cluster trees. For the mixed direct approach both variants are needed.

Before giving details how to apply the FMM in case of the poroelastodynamic problem, the Chebyshev interpolation with order p of an arbitrary function $f : \mathbb{R} \rightarrow \mathbb{C}$ is briefly summarized

$$f(x) \approx \sum_{m=1}^p S_p(\bar{x}_m, x) f(\bar{x}_m). \quad (21)$$

The interpolation function $S_p(\bar{x}_m, x)$ is defined on the interval $[-1, 1]$ with

$$S_p(\bar{x}_m, x) = \frac{1}{p} + \frac{2}{p} \sum_{n=1}^{p-1} T_n(x) T_n(\bar{x}_m) \quad \forall x \in [-1, 1]. \quad (22)$$

The extension to arbitrary intervals is performed by a linear transformation. For the sake of brevity, here, the necessary transformations are skipped in the formulas. $T_p(x)$ denotes the Chebyshev polynomial of order p

$$T_p(x) = \cos(p \arccos(x)) \quad \forall x \in [-1, 1], \quad (23)$$

and \bar{x}_m the corresponding roots

$$\bar{x}_m = \cos\left(\frac{(m - \frac{1}{2})\pi}{p}\right). \quad (24)$$

The extension to functions on \mathbb{R}^3 is made by an interpolation in each dimension, i.e.,

$$S_p(\bar{\mathbf{x}}_{\mathbf{m}}, \mathbf{x}) = \prod_{i=1}^3 S_p(\bar{x}_{m_i}, x_i), \quad (25)$$

with $\bar{\mathbf{x}}_{\mathbf{m}} = (\bar{x}_{m_1}, \bar{x}_{m_2}, \bar{x}_{m_3})$ and \mathbf{m} is a multi-index. The straightforward way to approximate non-scalar functions like the tensor-valued fundamental solution $\mathbf{U}(\mathbf{x}, \mathbf{y})$ is to interpolate all entries using the same interpolation scheme, which is equivalent to multiply the whole block with the scalar interpolation function S_p .

For the subsequent application of this interpolation one property is missing. It will be necessary to have the first derivative of the Chebyshev polynomial. A straight forward partial differentiation of (25) results in

$$\frac{\partial}{\partial x_k} S_p(\bar{\mathbf{x}}_{\mathbf{m}}, \mathbf{x}) = \frac{2}{p} \sum_{n=1}^{p-1} n U_{n-1}(x_k) T_n(\bar{x}_m) \prod_{\substack{i=1 \\ k \neq i}}^3 S_p(\bar{x}_{m_i}, x_i), \quad (26)$$

with the Chebyshev polynomial of second kind $U_n(x) = \sin((n+1)\arccos(x))/\sqrt{1-x^2}$.

After these preliminaries concerning the interpolation of the kernel function to get a low rank representation, the FMM can be formulated. Here, only the differences between the standard FMM and the FMM-BEM are discussed. Hence, the description of the multilevel scheme is omitted and can be found in [22]. It may be remarked that the interpolation and antinterpolation techniques as discussed in [21] can be used here as well. Hence, the M2L-operation can take advantage of the multilevel formulation. To illustrate the method the SLP approach is used, i.e., the matrix block V_{ij} in (17) is considered. Note, V_{ij} is called matrix block because this entry of the system matrix consists of the four by four block of the fundamental solution $\mathbf{U}(\mathbf{x}, \mathbf{y})$. The low rank approximation of this matrix of kernels is obtained by interpolation both variables \mathbf{x} and \mathbf{y}

$$(\mathbf{U}(\mathbf{x}, \mathbf{y}))^\top \approx \sum_{\mathbf{n}} S_p(\mathbf{x}, \bar{\mathbf{x}}_{\mathbf{n}}) \sum_{\mathbf{m}} (\mathbf{U}(\bar{\mathbf{x}}_{\mathbf{n}}, \bar{\mathbf{y}}_{\mathbf{m}}))^\top S_p(\bar{\mathbf{y}}_{\mathbf{m}}, \mathbf{y}) . \quad (27)$$

As mentioned above, the tensorial kernel function is interpolated using the same interpolation scheme for all 16 entries, which is equivalent to multiplying the whole block with the scalar interpolation function S_p . This fact allows to use the interpolation and antinterpolation in the upward and downward passes of the multilevel scheme. The points $\bar{\mathbf{x}}_{\mathbf{n}}, \bar{\mathbf{y}}_{\mathbf{m}}$ are the three-dimensional Chebyshev nodes transformed to the bounding box. This representation of the kernel shows clearly the separation of the two variables in a product of functions. Inserting this low rank representation in the matrix block V_{ij} results in

$$\mathbf{V}_{ij} \approx \underbrace{\sum_{\mathbf{n}} S_p(\mathbf{x}_i, \bar{\mathbf{x}}_{\mathbf{n}})}_{\text{L2P-operator}} \underbrace{\sum_{\mathbf{m}} (\mathbf{U}(\bar{\mathbf{x}}_{\mathbf{n}}, \bar{\mathbf{y}}_{\mathbf{m}}))^\top}_{\text{M2L-operator}} \underbrace{\int_{\text{supp}(\phi_j^0)} S_p(\bar{\mathbf{y}}_{\mathbf{m}}, \mathbf{y}) \phi_j^0(\mathbf{y}) d\mathbf{s}_{\mathbf{y}}}_{\text{P2M-operator}} . \quad (28)$$

Below the three expressions in (28) the usual abbreviations are put to have the link to the FMM multilevel schema. Obviously, using such an interpolation, the number of kernel evaluations can be reduced if the submatrix associated with the corresponding clusters of \mathbf{x}_i and ϕ_j^0 is larger than the associated M2L-operator of size $p^3 \times p^3$. The reduction is actually significantly larger, since for the numerical integration in the standard BEM (17) the kernel is evaluated for each quadrature point. Using the FMM this integration arises in the P2M-operator, which involves only the numerical integration of a polynomial. Especially in poroelastodynamics, this effects is pronounced as the exact kernel function is an expensive to compute function.

Next, the FMM version for the DLP, i.e., for

$$\mathbf{K}_{ij} = \int_{\text{supp}(\phi_j^1)} (\mathcal{T}_{\mathbf{y}} \mathbf{U}(\mathbf{x}_i, \mathbf{y}))^\top \phi_j^1(\mathbf{y}) d\mathbf{s}_{\mathbf{y}} , \quad (29)$$

has to be realized with an interpolated kernel. The traction fundamental solution $\mathcal{T}_{\mathbf{y}} \mathbf{U}$ depends on the normal vector of an associated surface, i.e., on the normal vector of the element to be integrated. Hence, a direct interpolation as in (27) is not possible. However, if the interpolation is applied on \mathbf{U} exactly as in (27) and the traction operator is applied on this low rank

	$K [\frac{N}{m^2}]$	$G [\frac{N}{m^2}]$	$\rho [\frac{kg}{m^3}]$	ϕ	$R [\frac{N}{m^2}]$	$\rho_f [\frac{kg}{m^3}]$	α	$\kappa [\frac{m^4}{Ns}]$
rock	$8 \cdot 10^9$	$6 \cdot 10^9$	2458	0.19	$4.7 \cdot 10^8$	1000	0.867	$1.9 \cdot 10^{-10}$

Table 1: Material data of Berea sandstone (rock) [26]

representation, anything works out. The interpolation with respect to \mathbf{y} gives then

$$\mathbf{K}_{ij} \approx \sum_{\mathbf{m}} (\mathbf{U}(\mathbf{x}_i, \bar{\mathbf{y}}_{\mathbf{m}}))^{\top} \int_{supp(\phi_j^1)} \mathcal{T}_y^{\top} S_p(\bar{\mathbf{y}}_{\mathbf{m}}, \mathbf{y}) \phi_j^1(\mathbf{y}) d\mathbf{s}_{\mathbf{y}}, \quad (30)$$

i.e., the traction operator \mathcal{T}_y is shifted onto the interpolation functions. This leads to a tensorial interpolation operator, whereas all other operations are identical to the SLP and the explicit expression is

$$\mathbf{K}_{ij} = \underbrace{\sum_{\mathbf{n}} S_p(\mathbf{x}_i, \bar{\mathbf{x}}_{\mathbf{n}})}_{\text{L2P-operator}} \underbrace{\sum_{\mathbf{m}} (\mathbf{U}(\bar{\mathbf{x}}_{\mathbf{n}}, \bar{\mathbf{y}}_{\mathbf{m}}))^{\top}}_{\text{M2L-operator}} \underbrace{\int_{supp(\phi_j^0)} \mathcal{T}_y^{\top} S_p(\bar{\mathbf{y}}_{\mathbf{m}}, \mathbf{y}) \phi_j^0(\mathbf{y}) d\mathbf{s}_{\mathbf{y}}}_{\text{P2M-operator}}. \quad (31)$$

Hence, the calculation of the far field of the DLP-operator only involves the evaluation of the fundamental solution \mathbf{U} itself.

The above given formulas for the SLP and DLP approach can be combined to establish an FMM version of the direct approach (20). As remarked above, the L2P- and M2L-operator can be used for both, \mathbf{V}_{ij} and \mathbf{K}_{ij} , which are both involved in the direct approach. Last, to save storage the M2L-operator can be compressed by the SVD [21].

4 Numerical examples

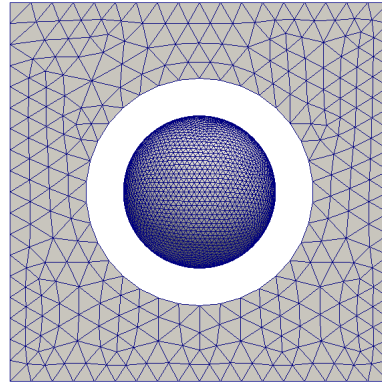
In this section, two numerical examples are presented. First, a cavity in a poroelastic domain is solved, where it is shown that the proposed method is suitable to solve engineering problems. Second, a convergence study is presented to show numerically the behavior of the method.

4.1 Cavity in a poroelastic medium

A cavity in a poroelastic material is considered. The cavity is modelled as a sphere with radius 1 m and the material data of a rock (Berea sandstone, see Tab. 1) are chosen. The boundary conditions are prescribed total tractions in the x -direction with magnitude one and a prescribed normal flux of the same magnitude. Hence, a pure Neumann problem is given. The integral equation (20) reduces to

$$(\mathbf{C}_{NN} + \mathbf{K}_{NN}) \mathbf{u}_N^g = \mathbf{V}_{NN} \mathbf{g}_N. \quad (32)$$

Due to the radiation condition this problem has a unique solution. The proposed FMM is applied on this equation. The geometry and the used mesh are given in Fig. 1. Additionally to the mesh of the sphere, a screen for displaying the solid displacements and the pore pressure is



elements	7648
nodes	3826
Frequency	2000 Hz
FMM order	5
FMM level	4

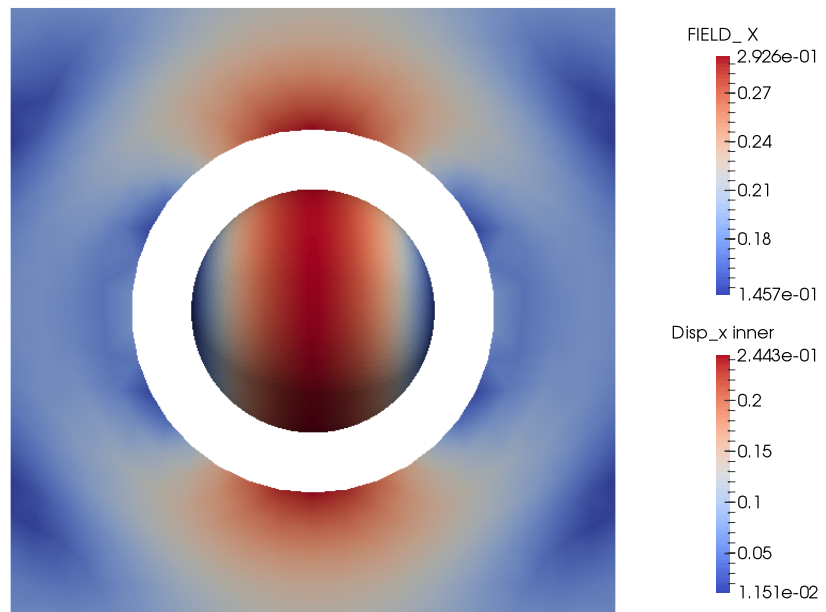
Figure 1: Spherical cavity in a poroelastic material: Geometry and mesh on the sphere and the screen used for inner points calculations

sketched in Fig. 1. The depicted elements on the screen are only used to define the points for the post processor. A problem in frequency domain is treated, i.e., the Laplace parameter s is pure imaginary. A frequency of 2000 Hz ($s = (0 + 12566i) s^{-1}$) is applied, which can easily be handled by the given mesh density with a mesh width of $h = 0.0625$ m. In Fig. 2, the absolute values of the solid displacements in direction of the load and the pore pressure are displayed on the sphere and in the interior of the medium. The results for the sphere and at the interior points have been scaled differently to have a better view on the results. Both legends are given, where the word ‘inner’ indicates the scale for the solutions on the screen. The solutions show a symmetric picture, which is in accordance with the problem. Note, the solutions are complex valued and in the figures the absolute value, i.e., the amplitude, is given.

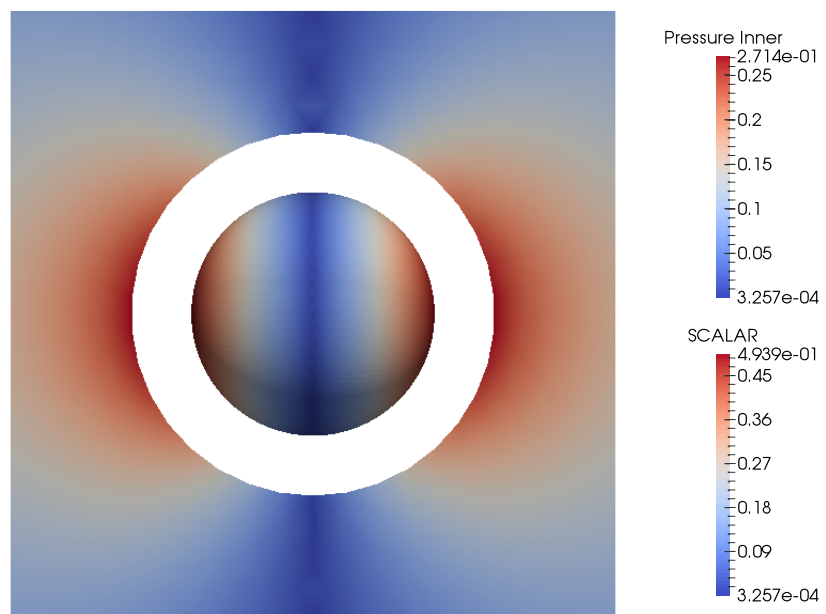
To access the accuracy of the presented results a computation has been made with a normal dense BEM. The problem is small enough such that a dense computation is possible with the available hardware. A pointwise ℓ_2 -error

$$\text{err}_{rel}(\mathbf{u}) = \sqrt{\frac{\sum |\mathbf{u}^{FMM} - \mathbf{u}^{dense}|^2}{\sum |\mathbf{u}^{dense}|^2}} \quad \text{err}_{rel}(p) = \sqrt{\frac{\sum |p^{FMM} - p^{dense}|^2}{\sum |p^{dense}|^2}} \quad (33)$$

has been computed at all nodes either on the sphere or in the interior. The superscripts *FMM* and *dense* denote the solutions from the respective computation with the FMM or dense BEM. These errors are plotted versus the expansion order of the FMM in Fig. 3. It is clearly observed that the error decreases exponentially as it can be expected for the Chebyshev expansion of the smooth part of the kernel function. On the contrary, the efficiency measured in the compression rate increases from 5% to 14%, i.e., the higher expansion order requires more storage. In [45], it has been shown that it increases with $O(p^6)$, which is caused by the M2L-operator with size $p^3 \times p^3$. However, the introduced SVD to compress the M2L-operator saves storage. Essentially, in this example the M2L-operator is compressed approximately by 50% for $p = 3$ up to 7% for $p = 6$. It must be remarked that the latter increases the computing time but significantly saves storage. All results presented above have been computed with a multilevel schema with $L = 4$.



(a) Solid displacement in x-direction (absolute value)



(b) Pore pressure (absolute value)

Figure 2: Solid displacements and pore pressure at 2000Hz

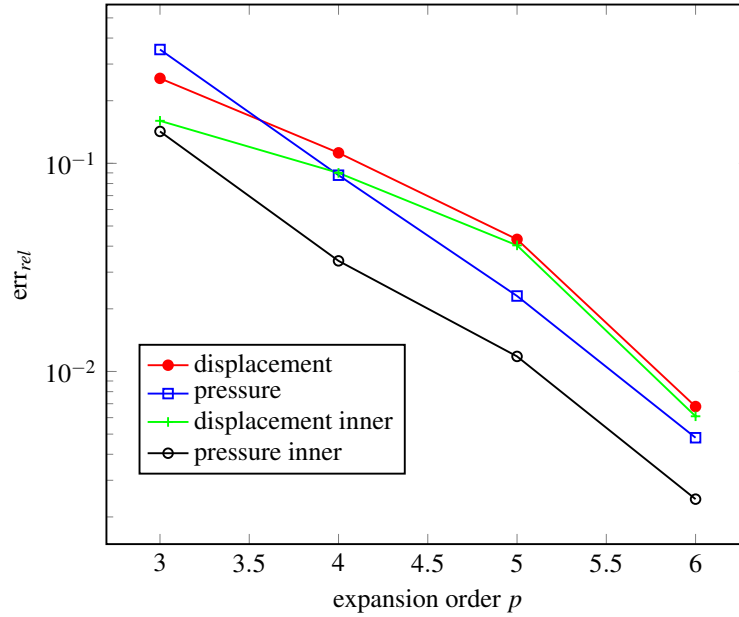


Figure 3: Error of displacements and pore pressure versus the expansion order p

A smaller value has produced slightly larger errors, whereas an increasing to $L = 6$ has the same errors but need more computing time. It seems that for this relatively small example $L = 4$ is the best choice.

4.2 Convergence studies

Next, the FMM-BEM for the poroelastic problem is tested with a given numerical solution of the homogenous differential equation. To study a general case, the calculation domain is a unit cube which is rotated along the axes of the coordination system (see Fig. 4). Setting a source point outside the cube, the individual rows of the fundamental solution $\mathbf{U}(\mathbf{x}, \mathbf{y})$ fulfil the homogeneous governing equations (1). A linear combination of all rows is used as boundary condition. Hence, the solution in the domain is as well the fundamental solution. Here, the source point is set to $\mathbf{y}_S = (0.6, 0.6, 0.6)^\top$. The complex frequency is set to $s = (3000 + 5000i) s^{-1}$ and, as above, the material data of Berea sandstone are assumed (see Tab. 1). The initial velocity of the fast compressional wave is $\approx 2846 \text{ m/s}$ for these material data, which gives an approximate wave number of 1.8. The principal behavior of the proposed FMM does not change for different complex frequencies. Tests have been made with $s = (1 + 2i) s^{-1}$ and $s = (3000 + 10000i) s^{-1}$, i.e., quasi-static conditions and a doubled wave number of ≈ 3.6 . In these test the same behavior as reported in the following have been observed with different error levels but with no need for different parameters of the FMM. It can be speculated that a frequency exists, where the FMM may be modified, e.g., by introducing a directional clustering.

The Dirichlet problem is solved with the SLP and DLP ansatz. To test the mixed direct formulation (20) on three sides of the cube a Dirichlet boundary condition and on the other sides a Neumann boundary condition is prescribed. The latter can be computed from the fundamental

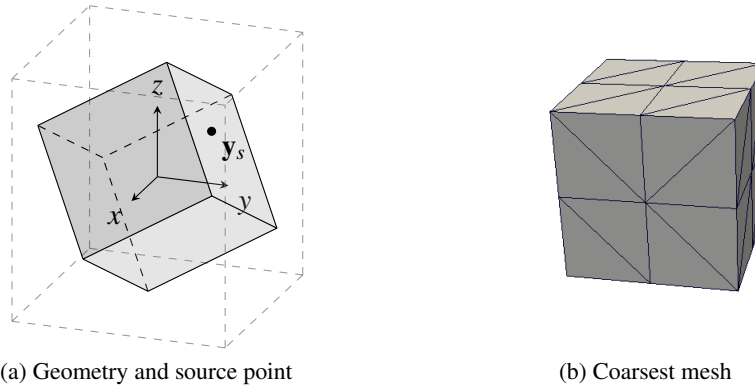


Figure 4: Geometry and orientation of the cube with the coarsest mesh

Mesh	dofs SLP	dofs DLP	dofs mixed
1	192	104	100
2	768	392	420
3	3072	1544	1732
4	12288	6152	7044
5	49152	24584	28420
6	196608	98312	114180
7	786432	393224	457732

Table 2: Parameter of used meshes

solution $\mathbf{U}(\mathbf{x}, \mathbf{y})$ by applying the traction operator (6). A sequence of triangulations by global uniform refinement starting at the coarsest discretization using 48 elements is produced. This mesh is displayed in Fig. 4 and the respective numbers of dofs are given in Tab. 2. For each refinement level of the mesh the number of elements N times 4 (three displacements/tractions and one pressure/flux dofs) is given in the column of the SLP as in this case constant shape functions are used. The column of the DLP is essentially 4 times the number of nodes. The last column gives the dofs for the mixed problem (20), which determine the size of the matrix on the left hand side in this equation.

The computation parameters for the multilevel FMM, i.e., the number of levels L and the polynomial order p are given in Tab. 3. The M2L-operators are compressed by a SVD with ϵ_{SVD} as given in Tab. 3. The value of ϵ_{SVD} has been adjusted such that the overall error is not influenced, i.e., the other errors are dominating. As solver a GMRes with a diagonal preconditioner has been used. The precision of the iterative solver has been set to $\epsilon_{\text{GMRes}} = 10^{-6}$. The respective iteration numbers N_{it} are listed in Tab. 3. The mixed problem is solved with a Schur-complement, which results in a nested GMres solve. Hence, three iteration numbers are given in Tab. 3, which corresponds to the inner solve and the outer solve for the generalized displacements \mathbf{u}^g and the last number is for the generalized traction solution \mathbf{t}^g . Obviously, for the SLP a better preconditioner should be found as these numbers grow dramatically with the size of the problem. This effect

Mesh	SLP				DLP				mixed			
	L	p	ϵ_{SVD}	N_{it}	L	p	ϵ_{SVD}	N_{it}	L	p	ϵ_{SVD}	N_{it}
1	2	2	10^{-3}	17	2	2	10^{-3}	8	2	2	10^{-3}	11-24-11
2	2	3	10^{-3}	20	2	2	10^{-3}	10	2	2	10^{-3}	13-26-14
3	3	4	10^{-4}	26	2	5	10^{-3}	11	3	3	10^{-3}	17-26-19
4	4	5	10^{-4}	35	3	6	10^{-3}	13	4	4	10^{-4}	23-26-24
5	5	5	10^{-4}	46	4	6	10^{-3}	14	5	6	10^{-5}	30-26-31
6	6	6	10^{-4}	59	5	7	10^{-5}	15	6	6	10^{-5}	41-26-40
7	7	7	10^{-5}	77	6	8	10^{-5}	15	7	7	10^{-5}	53-27-49

Table 3: Computation parameters

is also seen in the iteration numbers for the mixed problem, where only the middle number is nearly constant, which corresponds to a solution with the DLP.

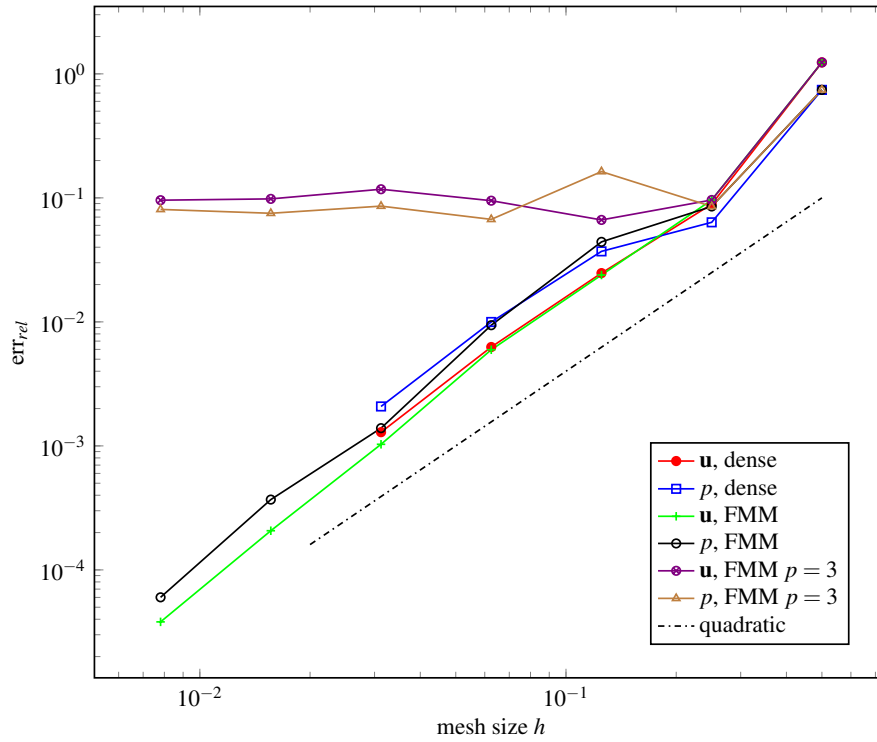
The polynomial order p has been chosen such that the error is comparable to a dense computation, i.e., a poroelastodynamic BEM without the FMM. For the SLP and DLP calculations the error is measured as mean value of the L_2 -error at 27 points inside the domain. These points are located at a cube centered at the midpoint with side length of 0.02m. The level L of the multilevel FMM, i.e., the depth of the octree, is determined by experience and analogously as in the elastodynamic case [45].

The expected convergence orders are the same as for the Laplacian (c.f. the proofs in poroelastodynamics [46]), i.e., quadratic for the solution at interior points. Note, a collocation method is used here and, consequently, the cubic order at inner points can not be expected. Both, the dense and the FMM results show this expected behavior. In Fig. 5, the relative L_2 -error is plotted versus the mesh size for the SLP and for the DLP. Additionally to the graphs for the FMM using the parameters from Tab. 3, results for a constant interpolation order $p = 3$ for the SLP and $p = 4$ for the DLP are added. These lines show that from a distinct error level on the FMM-error dominates and the convergence is no longer ensured. However, the error stays at a constant level and is essentially the interpolation error. For a suitable parameter set the convergence order of the FMM and the dense results coincide not only in the tendency but also in size. This proves that the error introduced by the FMM is smaller than the approximation error of the BEM.

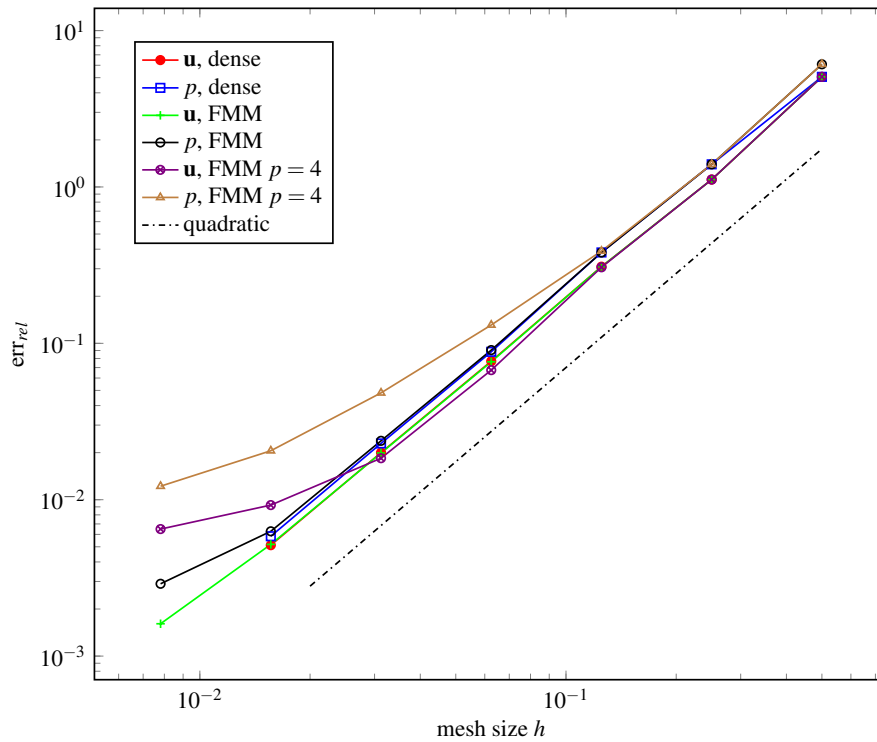
For the mixed problem the direct formulation (20) is applied. The error measure is

$$\text{err}_{abs} = \|\mathbf{u}(\mathbf{x}) - \mathbf{u}_h(\mathbf{x})\|_{L_2(\Gamma)} \quad \text{err}_{rel} = \frac{\text{err}_{abs}}{\|\mathbf{u}(\mathbf{x})\|_{L_2(\Gamma)}} \quad \forall \mathbf{x} \in \Gamma, \quad (34)$$

where $\|\cdot\|_{L_2(\Gamma)}$ denotes the spatial L_2 -norm on the boundary. The integration is numerically evaluated with a Gauss-quadrature. The approximated BE solution is denoted with \mathbf{u}_h , whereas \mathbf{u} means the exact solution. For the other physical quantities this error definition applies analogously. It can be expected that the Dirichlet data show a quadratic convergence order and the Neumann data a linear. In Fig. 6, the relative L_2 -error is plotted versus the mesh size. As in the test before, the FMM and the dense results show the same behavior with respect to the convergence order and the error size. The expected rates are obtained if the listed parameters for the FMM are used. Both tests show that the proposed FMM does not spoil the properties of the



(a) SLP



(b) DLP

Figure 5: Dirichlet problem with indirect BEM: Relative L_2 -error versus mesh width h

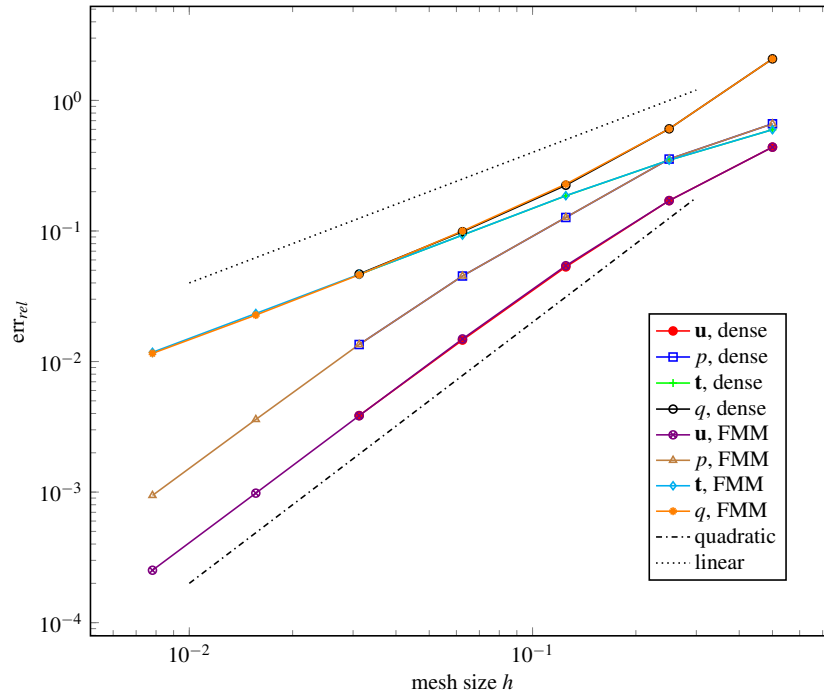


Figure 6: Mixed direct problem: Relative L_2 -error versus mesh width h

BE formulation as long as a sufficient order for the interpolation is used. Hence, the interpolation based FMM is robust in the sense that the error introduced is controllable, however, not determinable in advance.

It must be remarked that in both tests above, the dense calculation was not possible for the meshes 6 and 7 due to limited storage. One of the advantages of an FMM formulation is a reduced complexity and storage. It can be expected that the storage is almost linear with an logarithmic term. In Fig. 7, the storage in *GB* is plotted versus the degrees of freedom. For the dense formulation the quadratic growth in storage is clearly visible. The FMM formulation has in the beginning as well a quadratic growth, but asymptotically the almost linear tendency can be observed. Obviously, the storage can be reduced if the interpolation order is not increased with increasing numbers of dofs. But this does not change the order, only the factor. This might be relevant for real world engineering calculations where the problem itself produces a large amount of dofs and the precision is already limited by the material data or the model itself. The presented results show as well that for small sized problems the FMM has an overhead and requires even more storage. The 'turn over point' seems to be above 10^4 dofs, which is significantly higher compared to scalar problems like the Helmholtz equation. This 'turn over point' might be shifted to smaller values by some programming tricks or using some symmetries in the fundamental solution.

The second important aspect is the complexity. Here, no complexity analysis is made as it can be assumed that it is not different to the elastodynamic case. However, a study on the CPU-time may show the principal behavior. Certainly, the absolute CPU time is not representative as

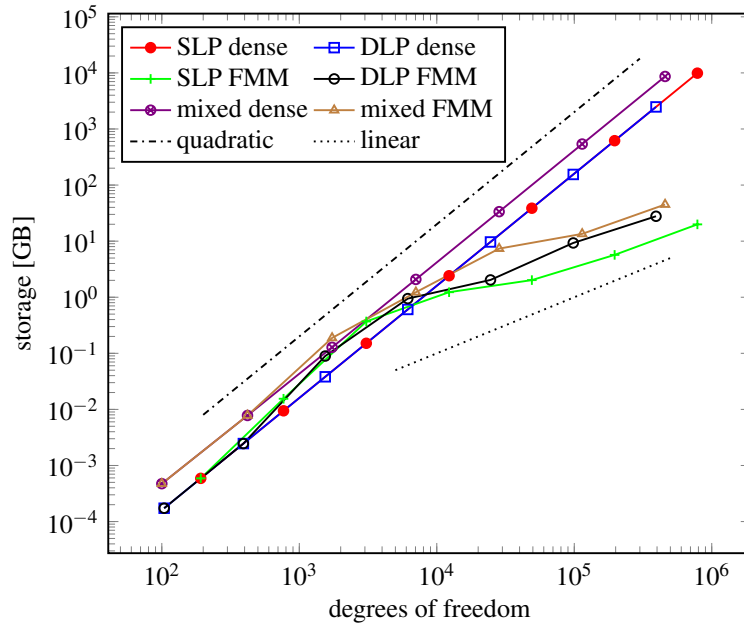


Figure 7: Storage of FMM and the dense BEM in GB

compiler, programming, CPUs, etc influence the absolute value. Here, only the tendency in the comparison with the dense formulation is presented. All computations have been performed on one node with 64 cores and 256 GB memory. The process was the only process on this node of the cluster at TU Graz. Parallelisation has been done with OpenMP and for both, the FMM and the dense computations, the same parallel routine to compute the matrix entries has been used. Hence, the CPU times of the dense calculation and of the FMM are comparable. Further, the iteration numbers of the iterative solver may disturb this study. That is why not a full BE calculation but only the time for one matrix-vector product is presented in Fig. 8. The arbitrarily chosen vector for these matrix-vector products is a unit vector. The results displayed are for the single layer potential. Those for the double layer potential are similar but larger. Beside the timings for the dense calculation those for three different FMM calculations are presented. The line denoted with *SLP FMM (SVD)* uses the levels and interpolation orders as given in Tab. 3 and has SVD compressed M2L-operators. The line *SLP FMM* has the same setting but no compression of the M2L-operators. The third FMM calculation *SLP FMM $p = 3$* uses a constant interpolation order with compressed M2L-operators and the levels given in Tab. 3. The quadratic growth of the dense calculation can be observed (dash-dotted line). The FMM shows asymptotically a log-linear behavior, where the logarithmic term has a power of six (dotted line). This is similar to the behavior of the elastodynamic case where this exponent has been shown in a complexity analysis [45]. A linear behavior is obtained for the case of constant polynomial order. The results in Fig. 8 show as well that the SVD compression of the M2L-operators takes time but for larger dofs it becomes less and less dominant. Overall, the 'turn over point' where the FMM becomes faster compared to a dense calculation is above 10^4 dofs.

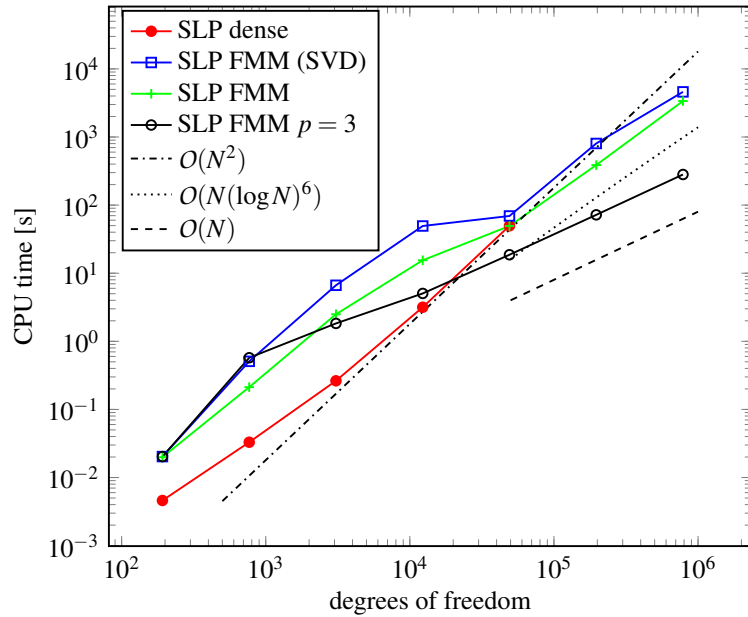


Figure 8: Timings: CPU-time for one matrix-vector product of the FMM and the dense BEM in seconds

5 Conclusions

The poroelastodynamic BEM in Laplace- or frequency domain is well established. For the u - p -formulation four degrees of freedom per node are required. This fact and the quadratic complexity of a standard approach using an iterative solver does not allow to compute even medium sized problems in 3D. Fast methods have been developed for BE formulations, which reduces the complexity to almost linear order. Here, the fast multipole method (FMM) is applied to reduce the complexity of the poroelastodynamic BEM also to an almost linear order. Due to the complicated fundamental solutions a black-box type FMM is preferable.

The presented black-box FMM-BEM uses the Chebyshev interpolation-based FMM. This, firstly, reduces the number of evaluations of the computationally expensive fundamental solution significantly. Secondly, for large problems, the storage requirement of the FMM-BEM operators is almost linear. A significant compression, though, was only achieved using the SVD to compress the M2L-operators. In the tests, asymptotically, a log-linear behavior with respect to the CPU-time has been observed. It must be remarked that the iterative solver works only if the problem is transformed to dimensionless variables. The presented results show that the proposed FMM can be adjusted such that the convergence rates of the standard BEM can be obtained. For high frequencies adjustments or different FMM techniques may be necessary. The presented results are restricted to the low frequency range. Another open point of the proposed method is to formulate an effective preconditioner to reduce the iteration numbers. However, this is independent of the proposed FMM.

Acknowledgement The author gratefully acknowledges the financial support by the Austrian Science Fund (FWF) under Grant P 24800-N26. Most of the programming work has been performed by Thomas Traub, which is also gratefully acknowledged.

References

- [1] B. Alpert, G. Beylkin, R. Coifman, and V. Rokhlin. Wavelet-like bases for the fast solutions of second-kind integral equations. *SIAM J. Sci. Comput.*, 14(1):159–184, 1993.
- [2] M. Bebendorf. Approximation of boundary element matrices. *Numer. Math.*, 86(4):565–589, 2000.
- [3] M. Bebendorf and R. Grzhibovskis. Accelerating Galerkin BEM for linear elasticity using adaptive cross approximation. *Math. Meth. Appl. Sci.*, 29(14):1721–1747, 2006.
- [4] M. Bebendorf and S. Rjasanow. Adaptive low-rank approximation of collocation matrices. *Computing*, 70:1–24, 2003.
- [5] M. A. Biot. General theory of three-dimensional consolidation. *J. Appl. Phys.*, 12(2):155–164, 1941.
- [6] M. A. Biot. Theory of elasticity and consolidation for a porous anisotropic solid. *J. Appl. Phys.*, 26(2):182–185, 1955.
- [7] M. A. Biot. Theory of propagation of elastic waves in a fluid-saturated porous solid.I. Low-frequency range. *J. Acoust. Soc. Am.*, 28(2):168–178, 1956.
- [8] M. A. Biot. Theory of propagation of elastic waves in a fluid-saturated porous solid.II. Higher frequency range. *J. Acoust. Soc. Am.*, 28(2):179–191, 1956.
- [9] M. A. Biot. Theory of deformation of a porous viscoelastic anisotropic solid. *J. Appl. Phys.*, 27(5):459–467, 1956.
- [10] G. Bonnet. Basic singular solutions for a poroelastic medium in the dynamic range. *J. Acoust. Soc. Am.*, 82(5):1758–1762, 1987.
- [11] G. Bonnet and J.-L. Auriault. Dynamics of saturated and deformable porous media: Homogenization theory and determination of the solid-liquid coupling coefficients. In N. Boccara and M. Daoud, editors, *Physics of Finely Divided Matter*, pages 306–316. Springer Verlag, Berlin, 1985.
- [12] S. Chaillat, M. Bonnet, and J.-F. Semblat. A multi-level fast multipole BEM for 3-D elastodynamics in the frequency domain. *Comput. Methods Appl. Mech. Engrg.*, 197(49–50):4233–4249, 2008.
- [13] J. Chen and G. F. Dargush. Boundary element method for dynamic poroelastic and thermoelastic analysis. *Internat. J. Solids Structures*, 32(15):2257–2278, 1995.

- [14] A. H.-D. Cheng, T. Badmus, and D.E. Beskos. Integral equations for dynamic poroelasticity in frequency domain with BEM solution. *J. Engrg. Mech., ASCE*, 117(5):1136–1157, 1991.
- [15] R. de Boer. *Theory of Porous Media*. Springer-Verlag, Berlin, 2000.
- [16] S. Diebels and W. Ehlers. Dynamic analysis of a fully saturated porous medium accounting for geometrical and material non-linearities. *Int. J. Numer. Methods. Engrg.*, 39(1):81–97, 1996.
- [17] J. Domínguez. Boundary element approach for dynamic poroelastic problems. *Int. J. Numer. Methods. Engrg.*, 35(2):307–324, 1992.
- [18] W. Ehlers. Constitutive equations for granular materials in geomechanical context. In K. Hutter, editor, *Continuum Mechanics in Environmental Sciences and Geophysics*, CISM Courses and Lecture Notes, No. 337, pages 313–402. Springer-Verlag, Wien, 1993.
- [19] W. Ehlers. Compressible, incompressible and hybrid two-phase models in porous media theories. *ASME: AMD-Vol.*, 158:25–38, 1993.
- [20] S. Erichsen and S. A. Sauter. Efficient automatic quadrature in 3-d Galerkin BEM. *Comput. Methods Appl. Mech. Engrg.*, 157(3–4):215–224, 1998.
- [21] W. Fong and E. Darve. The black-box fast multipole method. *J. Comput. Phys.*, 228(23): 8712–8725, 2009.
- [22] L. Greengard and V. Rokhlin. A fast algorithm for particle simulations. *J. Comput. Phys.*, 73(2):325–348, 1987. ISSN 0021-9991. doi: 10.1016/0021-9991(87)90140-9. URL <http://www.sciencedirect.com/science/article/pii/0021999187901409>.
- [23] L. Greengard and V. Rokhlin. A new version of the Fast Multipole Method for the Laplace equation in three dimensions. *Acta Num.*, 6:229–269, 1997.
- [24] W. Hackbusch and Z. P. Nowak. On the fast matrix multiplication in the boundary element method by panel clustering. *Numer. Math.*, 54:463–91, 1989.
- [25] D. L. Johnson, J. Koplik, and R. Dashen. Theory of dynamic permeability and tortuosity in fluid-saturated porous media. *Journal of Fluid Mechanics*, 176:379–402, 1987. doi: 10.1017/S0022112087000727.
- [26] Y. K. Kim and H. B. Kingsbury. Dynamic characterization of poroelastic materials. *Exp. Mech.*, 19(7):252–258, 1979.
- [27] Y. Liu. *Fast Multipole Boundary Element Method: Theory and Applications in Engineering*. Cambridge University Press, Cambridge, New York, 2009.
- [28] C. Lubich. Convolution quadrature and discretized operational calculus. I. *Numer. Math.*, 52(2):129–145, 1988.

- [29] C. Lubich. Convolution quadrature and discretized operational calculus. II. *Numer. Math.*, 52(4):413–425, 1988.
- [30] G. D. Manolis and D. E. Beskos. Integral formulation and fundamental solutions of dynamic poroelasticity and thermoelasticity. *Acta Mech.*, 76(1-2):89–104, 1989. Errata [31].
- [31] G. D. Manolis and D. E. Beskos. Corrections and additions to the paper “Integral formulation and fundamental solutions of dynamic poroelasticity and thermoelasticity”. *Acta Mech.*, 83(3-4):223–226, 1990.
- [32] M. Messner and M. Schanz. A regularized collocation boundary element method for linear poroelasticity. *Comput. Mech.*, 47(6):669–680, 2011. doi: 10.1007/s00466-010-0569-y.
- [33] M. Messner and M. Schanz. A symmetric Galerkin boundary element method for 3d linear poroelasticity. *Acta Mech.*, 223(8):1751–1768, 2012. doi: 10.1007/s00707-012-0637-9.
- [34] M. Messner, M. Schanz, and E. Darve. Fast directional multilevel summation for oscillatory kernels based on Chebyshev interpolation. *J. Comput. Phys.*, 231(4):1175–1196, 2012. doi: 10.1016/j.jcp.2011.09.027.
- [35] N. Nishimura. Fast multipole accelerated boundary integral equation methods. *AMR*, 55(4):299–324, 2002.
- [36] G. Of, O. Steinbach, and W. L. Wendland. Applications of a fast multipole Galerkin boundary element method in linear elastostatics. *Comput. Vis. Sci.*, 8:201–209, 2005.
- [37] V. Rokhlin. Rapid solution of integral equations of classical potential theory. *J. Comput. Phys.*, 60:187–207, 1983.
- [38] M. Schanz. Application of 3-d Boundary Element formulation to wave propagation in poroelastic solids. *Eng. Anal. Bound. Elem.*, 25(4-5):363–376, 2001.
- [39] M. Schanz. *Wave Propagation in Viscoelastic and Poroelastic Continua: A Boundary Element Approach*, volume 2 of *Lecture Notes in Applied Mechanics*. Springer-Verlag, Berlin, Heidelberg, New York, 2001. doi: 10.1007/978-3-540-44575-3.
- [40] M. Schanz. Poroelastodynamics: Linear models, analytical solutions, and numerical methods. *AMR*, 62(3):030803–1–030803–15, 2009. doi: doi:10.1115/1.3090831.
- [41] M. Schanz and S. Diebels. A comparative study of Biot’s theory and the linear Theory of Porous Media for wave propagation problems. *Acta Mech.*, 161(3-4):213–235, 2003. doi: 10.1007/s00707-002-0999-5.
- [42] M. Schanz and L. Kielhorn. Dimensionless variables in a poroelastodynamic time domain boundary element formulation. *Building Research Journal*, 53(2-3):175–189, 2005.
- [43] M. Schanz, O. Steinbach, and P. Urthaler. A boundary integral formulation for poroelastic materials. *Proc. Appl. Math. Mech.*, 9(1):595–596, 2009. doi: 10.1002/pamm.200910269.

- [44] T. Takahashi, N. Nishimura, and S. Kobayashi. A fast BIEM for three-dimensional elastodynamics in time domain. *Eng. Anal. Bound. Elem.*, 28(2):165–180, 2004. Erratum in *EABEM*, 28, 165–180, 2004.
- [45] T. Traub. *A Kernel Interpolation Based Fast Multipole Method for Elastodynamic Problems*, volume 29 of *Computation in Engineering and Science*. Verlag der Technischen Universität Graz, 2016.
- [46] P. Urthaler. *Analysis of Boundary Element Methods for Wave Propagation in Poros Media*, volume 14 of *Computation in Engineering and Science*. Verlag der Technischen Universität Graz, 2012.
- [47] A. Verde and A. Ghassemi. Large-scale poroelastic fractured reservoirs modeling using the fast multipole displacement discontinuity method. *Int. J. Numer. Anal. Methods Geomech.*, 40(6):865–886, 2016. ISSN 1096-9853. doi: 10.1002/nag.2430. URL <http://dx.doi.org/10.1002/nag.2430>. NAG-14-0316.R1.
- [48] Th. Wiebe and H. Antes. A time domain integral formulation of dynamic poroelasticity. *Acta Mech.*, 90(1-4):125–137, 1991.